Applied Catalysis B: Environmental 331 (2023) 122703

Contents lists available at ScienceDirect

Applied Catalysis B: Environmental

journal homepage: www.elsevier.com/locate/apcatb

Low-Pt supported on MOF-derived $Ni(OH)_2$ with highly-efficiently electrocatalytic seawater splitting at high current density

Jianpeng Sun [a], Zisheng Zhang [b], Xiangchao Meng [a,*]

[a] Key Laboratory of Marine Chemistry Theory and Technology (Ministry of Education), College of Chemistry & Chemical Engineering, Ocean University of China, Qingdao, Shandong 266100, China
[b] Department of Chemical and Biological Engineering, Faculty of Engineering, University of Ottawa, Ottawa, Ontario K1N6N5, Canada

ARTICLE INFO

Keywords:
Electrocatalysts
$Pt/Ni(OH)_2$
O vacancy
Seawater hydrogen evolution
AEM tests

ABSTRACT

Developing highly effective and stable electrocatalysts are attractive but highly challenging for alkaline seawater splitting. Herein, using a simple method, we developed a novel MOF derived nanosheets-nanoparticle-structured $Pt2/Ni(OH)_2/NF$ catalyst. Benefiting from strong metal-support interaction (SMSI) of Pt-O-Ni bond at interface, the synergistic effect of Pt-O vacancies (Ov) sites and excellent superhydrophilic surface, catalyst delivered excellent catalytic activity in seawater splitting. The overpotential was 19 mV at 10 $mA{\cdot}cm^{-2}$, which surpassed the commercial 20% Pt/C. A photovoltaic cell yielded up to 13.5% STH conversion efficiency. Furthermore, the cell voltage at 10 $mA{\cdot}cm^{-2}$ for anion exchange membrane (AEM) seawater electrolyzer in our design with the $Pt2/Ni(OH)_2/NF$ cathode catalyst was merely 1.46 V. The energy consumption to produce 1 m^3 of H_2 at the current density of 200 $mA{\cdot}cm^{-2}$ was 3.8 kW·h, below that of NF= |NF (4.3 kW·h). Theoretical results showed that the localized charge density and electronic structure of $Ni(OH)_2$ can be significantly modulated upon SMSI at interface and Ov. And the synergistic effect of Pt-Ov sites can balance the adsorption and desorption of H* . Ov could achieve high-efficiency adsorption of H_2O and optimize hydrogen spillover from $Ni(OH)_2$ to Pt, leading to excellent HER activity. This study provided a light in rational construction of robust seawater-based electrocatalysts for seawater splitting.

1. Introduction

Seawater, as an alternative water resource for electrocatalytic hydrogen evolution has increasingly attracted attentions [1–3]. However, the complexity of seawater resulted in the low activity and instability of electrocatalysts when applied in seawater splitting [4–6]. Compared with fresh water, the large content of Cl^- in seawater may block the active sites, preventing adsorption of H* and then leading to slow HER kinetics [7,8]. Moreover, Cl^- may cause corrosion and gradual dissolution of electrocatalyst, leading to catalyst poisoning and poor catalytic stability [9,10]. Therefore, it is urgent to design and prepare a highly effective and stable electrocatalyst for seawater splitting to evolve H_2.

Layered double hydroxides (LDHs) such as $Ni(OH)_2$ exhibited promises in electrocatalytic water splitting [11–13]. Nevertheless, strong H* adsorption capacity on its surface prevented the release of hydrogen, which further limited the electrocatalytic activity [14]. Pt has been designed in highly-efficiently electrocatalytic hydrogen evolution [15,16]. Due to the weak interaction between 4d orbital of Pt and 2p orbital of oxygen in H_2O, the adsorption and dissociation of H_2O on Pt was poor, especially in alkaline aqueous solution [17,18]. Considering the sluggish HER kinetics in alkaline seawater, designing and engineering seawater-based nanomaterials interfaces by coupling low-Pt with $Ni(OH)_2$ is considered to be an effective method. Zhao et al. designed Pt decorated $Ni{-}Ni(OH)_2$ to enhance reaction kinetics, which delivered high electrocatalytic activity [19]. Zhang et al. also reported a robust $Pt/TiO_2/Ni(OH)_2$ nanosheet arrays, which showed good performance for high current density alkaline water electrolysis due to the synergistic effect of Pt and $TiO_2/Ni(OH)_2$ [20]. Although many interface engineering research has been used to design highly reactive electrocatalyst, few reports on coupling Pt with $Ni(OH)_2$ to construct an high stability seawater-based catalyst, which was mainly because the complex ionic environment is easy to destroy the active site of the in seawater. Recently, strong metal-support interaction (SMSI) in catalysts, as an effective behavior to enhance the stability, has attracted extensive attentions[21]. Especially, the construction of M-O-M (M = metal)

* Corresponding author.
E-mail address: mengxiangchao@ouc.edu.cn (X. Meng).

https://doi.org/10.1016/j.apcatb.2023.122703
Received 21 November 2022; Received in revised form 9 March 2023; Accepted 26 March 2023
Available online 31 March 2023

bonds at interface can protect active sites well, which made electrocatalysts keep good stability [22,23]. At present, metal−organic frameworks (MOFs) as templates have been widely studied for transition metal-based electrocatalysts due to their tunable nanostructures, and excellent porosities [24,25]. Using MOFs as templates or precursors of $Ni(OH)_2$ can inherit the inherent structural advantages of MOFs [26]. Meanwhile, the surface of MOF is easy to generate O vacancies (Ov) and form M-O-M bonds during the in-situ conversion process, which can effectively prevent its active site aggregation and then improving the stability of $Ni(OH)_2$ in alkaline seawater splitting [27–29]. Therefore, approaches to couple Pt and SMSI effect on MOF derived $Ni(OH)_2$ would be an useful strategy to further improve electrocatalytic activity and stability in alkaline seawater splitting.

Based on above discussions, we developed a novel MOF derived nanosheets-nanoparticle-structured $Pt2/Ni(OH)_2/NF$ catalyst. SMSI of Pt-O-Ni bond at interface, synergistic effect of Pt-O vacancies (Ov) sites and excellent superhydrophilic surface in $Pt2/Ni(OH)_2/NF$ promoted the electrocatalytic activity. Furthermore, cell voltage at 10 $mA{\cdot}cm^{-2}$ for the anion exchange membrane (AEM) seawater electrolyzer was only 1.46 V. The energy consumption to produce 1 m^3 of H_2 at the current density of 200 $mA{\cdot}cm^{-2}$ was 3.8 kW·h, below that of NF= |NF (4.3 kW·h). The mechanism of as-prepared sample in alkaline seawater splitting was explored based on both experimental and theoretical computation results.

2. Experimental section

2.1. Preparation of Ni-MOF/NF

In a typical synthesis process, $NiCl_2{\cdot}6\ H_2O$ (44 mg) and terephthalic acid (62 mg) were separately dispersed in N,N-Dimethylformamide (DMF, 16 mL), ethanol (1 mL) and deionized (DI) water (1 mL) under ultrasonication. And the mixture was transferred into an autoclave, and a piece of NF (2 cm × 2 cm) was vertically immersed into the solution, which was kept at 120 °C for 12 h. As-synthesized product was obained at 70 °C under vacuum for 12 h.

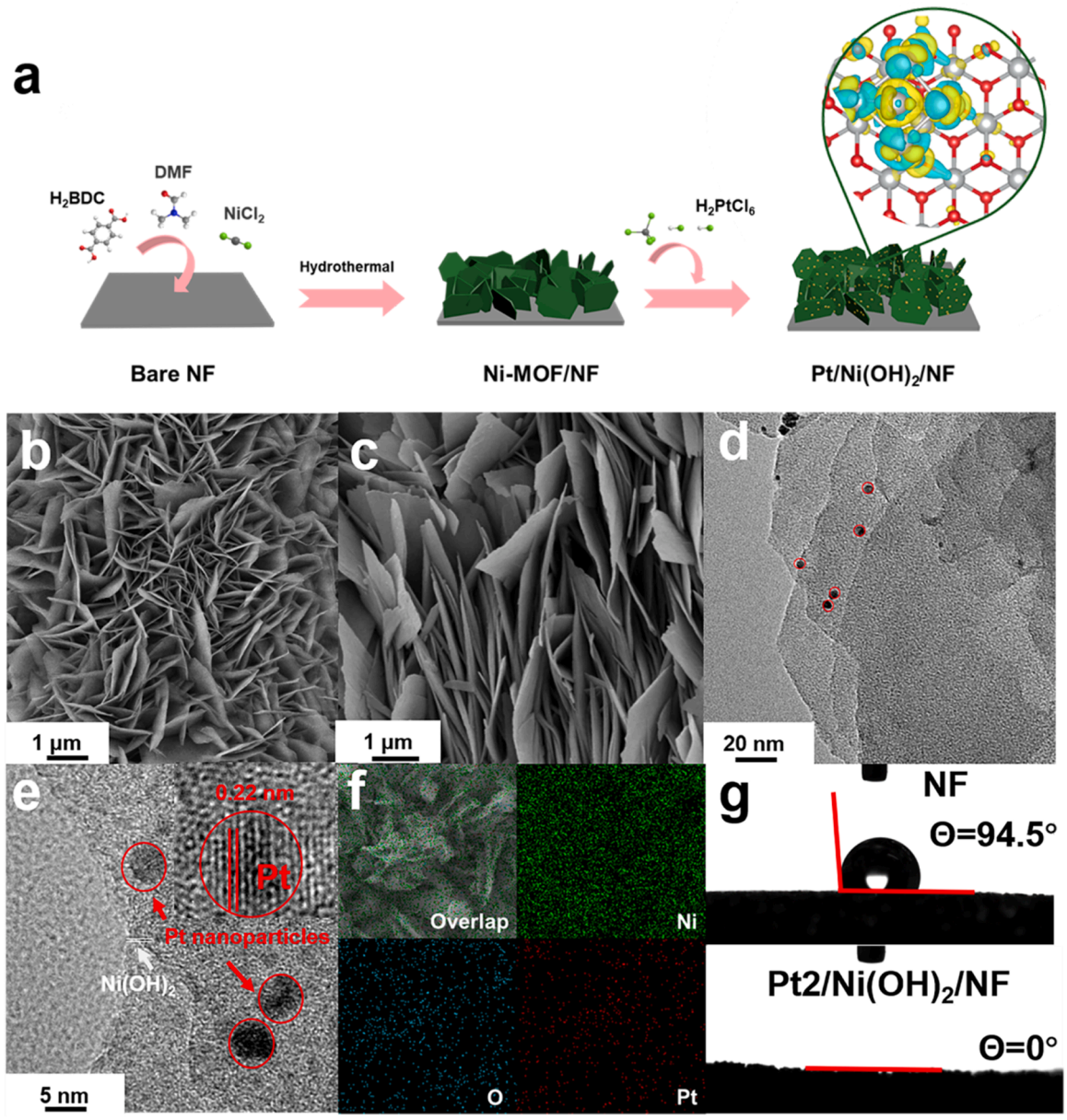

Fig. 1. (a) Schematic illustration of the synthesis of $Pt2/Ni(OH)_2/NF$. SEM images of (b) Ni-MOF/NF and (c) $Pt2/Ni(OH)_2/NF$. (d) TEM image, (e) HRTEM image and (f) EDS mapping images of $Pt2/Ni(OH)_2/NF$. (g) The droplet contact angle images of the bare NF and $Pt2/Ni(OH)_2/NF$.

2.2. Preparation of Pt/Ni(OH)$_2$/NF

A hydrothermal method was applied to prepare Pt/Ni(OH)$_2$/NF. Typically, H_2PtCl_6 (10 mg/mL: 240 μL, 480 μL and 720 μL) was dissolved in a Teflon-lined autoclave containing 15-mL DI water. And then a piece of Ni-MOF/NF (2 cm × 2 cm) was vertically immersed into the solution. Afterwards, the autoclave was kept at 150 °C for 460 min. Finally, Pt/Ni(OH)$_2$/NF was collected after washing.

3. Results and discussions

3.1. Synthesis and characterizations

Fig. 1a showed Ni-MOF-74 was chosen as a template to form Ni(OH)$_2$ due to their similar crystal structure (Fig. S1), and grown on NF using a hydrothermal method [30]. As-prepared Ni-MOF-74 was further treated to prepare Ni(OH)$_2$ using a alkaline hydrolysis at 150 °C (Fig. S1). From SEM and XRD tests (Fig. 1b and S2), Ni(OH)$_2$ was successfully constructed in NF. And then, Ni(OH)$_2$ was modified with three different amount of H_2PtCl_6. The content of Pt was calculated as 0.56%, 1.12% and 1.68 wt% in the composite, which was labelled as Pt1/Ni(OH)$_2$/NF, Pt2/Ni(OH)$_2$/NF and Pt3/Ni(OH)$_2$/NF, respectively. Pt2/Ni(OH)$_2$/NF maintained nanosheets morphlogy (Fig. 1c). TEM has been applied to investigate Pt in the composite in Figs. 1d and 1e. Pt nanoparticle had a fringe spacing of 0.22 nm, which was in consistent with the Pt [1 1 1] planes. And particles with a diameter of ~4 nm were found on nanosheets because of the SMSI of Pt-O-Ni bond at interface after in-situ MOF conversion process. From XRD patterns of Pt2/Ni(OH)$_2$/NF, peaks for Pt were also found, which were indexed in Fig. S3. In addition, the TEM image of pure Ni(OH)$_2$/NF was also tested in Fig. S4, and no particles were observed. Simultaneously, EDS mapping delievered the good distribution of O, Pt, Ni species (Fig. 1f and S5). Previous studies have been proved that the electrolyte ions were insufficiently adsorbed on the electrode surface, and the catalytic active sites could not be exposed to the maximum extent, resulting in poor electrocatalytic activity [31,32]. The construction of hydrophilic structure had a good effect on the catalytic reaction. And then, hydrophilicity of bare NF and Pt2/Ni(OH)$_2$/NF was investigated in Fig. 1g. Pt2/Ni(OH)$_2$/NF was superhydrophilic and had a contact angle closed to 0°, it was much smaller than that of NF substrate (94.5°), indicating that sites in Pt2/Ni(OH)$_2$/NF had good contact with electrolyte. Overall, Pt2/Ni(OH)$_2$/NF had good hydrophilicity and large specific surface area, which would accelerate the adsorption of electrolyte, and then achieving good electrocatalytic activity.

The compositions of as-prepared samples were investigated using XPS. The survey spectrum was depicted in Fig. S6, peaks for Ni, O, Pt and C were indexed, and no impre peaks were observed. The typical peaks of Ni^{3+} and Ni^{2+} were shown in Fig. 2a [33]. Compared with that of Ni(OH)$_2$/NF, peaks of Pt2/Ni(OH)$_2$/NF had a negatively shifts about ~0.41 eV, which meant electrons were accumulated at Ni species because of the formation of the strong metal-support interaction of Pt-O-Ni bond at interface after in-situ MOF conversion process in Pt2/Ni(OH)$_2$/NF [22]. The concentration of electrons could optimize the adsorption capacity of H* . And Pt-O-Ni bond at interface could protect

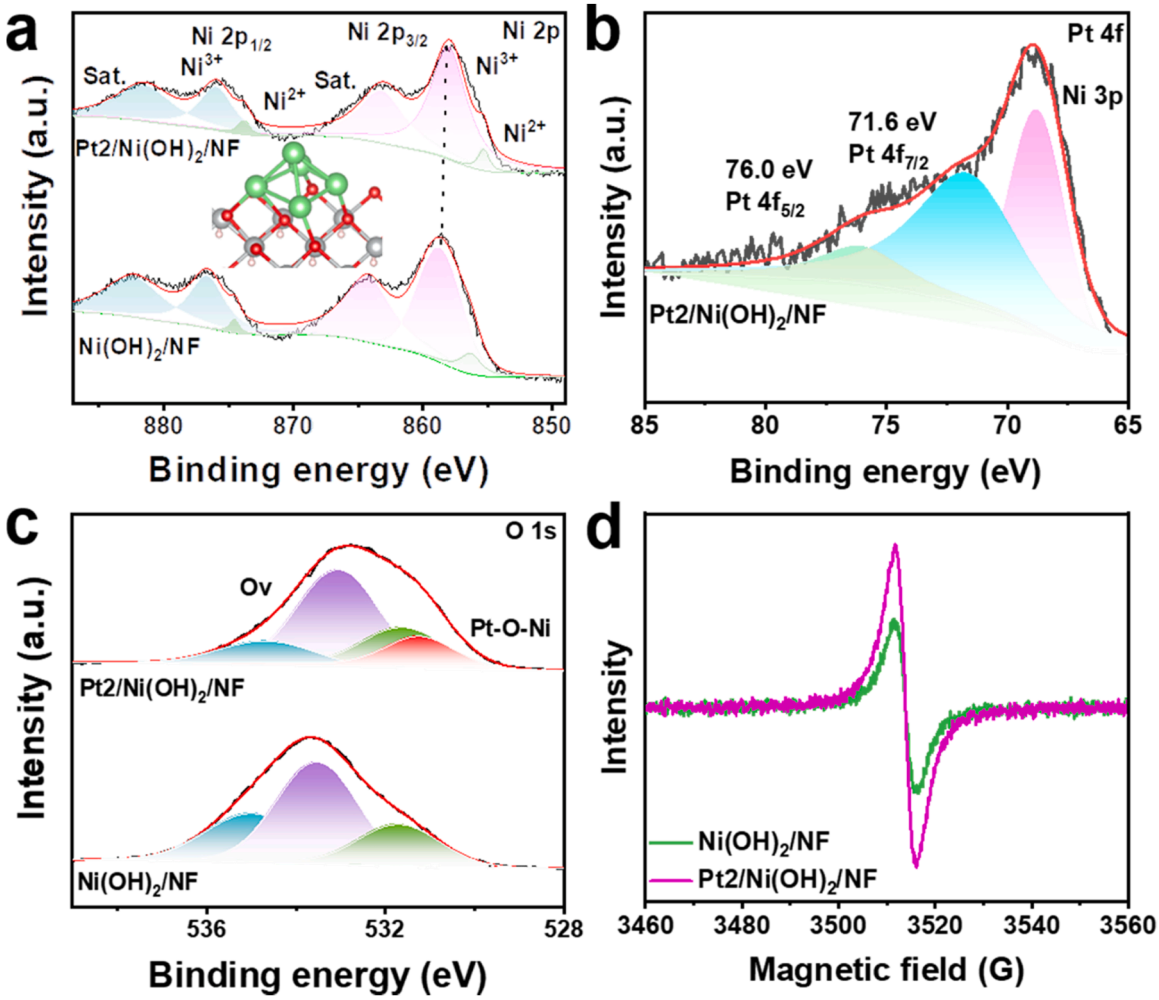

Fig. 2. XPS spectra of (a) Ni 2p, (b) Pt 4 f, (c) O 1 s (d) EPR spectra.

the active site during the electrocatalytic tests and make Pt2/Ni(OH)$_2$/NF maintain high reusability. Moreover, two characteristic peaks were indexed to Pt 4 $f_{7/2}$ and Pt 4 $f_{5/2}$ of Pt^{2+} species in Fig. 2b, which also implied the presence of a Pt–O–Ni structure [34]. SMSI between nanoparticles and Ni(OH)$_2$ could ensure its stable existence of Pt nanoparticles in HER process. Moreover, induced by the SMSI of Pt-O-Ni bond at interface, binding energy of lattice oxygen of Pt2/Ni(OH)$_2$/NF shifted to a lower level (531.6 eV) different from Ni(OH)$_2$/NF (531.7 eV) in Fig. 2c. And the peaks at 531.23 eV were ascribed to the Pt-O-Ni bond [34]. Meantime, the content of Ov in Pt2/Ni(OH)$_2$/NF also increased significantly from 50.47% to 54.99%. EPR spectra were shown to further verify the presence of Ov on Pt2/Ni(OH)$_2$/NF. Ni-MOF-74 readily formed Ov on Ni(OH)$_2$ at high temperatures (Fig. 2d). More importantly, more Ov in Pt2/Ni(OH)$_2$/NF were detected, which might be because the loaded Pt reduces the generation energy of Ov [35]. Overall, after forming Pt–O–Ni structure and Ov, electron structure has changed in Pt2/Ni(OH)$_2$/NF, which could enhance strong metal-support interaction and ensure its stable existence of active sites in alkaline seawater splitting.

3.2. Electrochemical HER performance

HER activities of Pt2/Ni(OH)$_2$/NF and other contrast samples were studied in alkaline seawater solution. Comparatively, Pt2/Ni(OH)$_2$/NF delievered a high activity (19 mV), which was pretty lower than bare NF (241 mV) and Ni(OH)$_2$/NF (186 mV) at 10 mA·cm^{-2} and even better than 20% Pt/C (21 mV) (Fig. 3a). Meantime, Pt2/Ni(OH)$_2$/NF only required HER overpotentials of 76 and 283 mV at 100 and 1000 mA cm^{-2}, respectively. As displayed in Fig. 3b, the Tafel value went from 189 mV·dec^{-1} for Ni(OH)$_2$/NF and 281 mV·dec^{-1} for NF to 70 mV·dec^{-1} for Pt2/Ni(OH)$_2$/NF after the Pt load, indicating that HER kinetics was enhanced for Ni(OH)$_2$ with Pt modification [36]. Moreover, Pt2/Ni(OH)$_2$/NF still showed excellent activity, which only needed 274 mV at 1000 mA cm^{-2} and had small Tafel value in 1.0 M KOH (Fig. S7). Such activity could be because: (i) Pt nanoparticles and Ov could effectively lower the adsorption of H* and then achieve high-efficiency adsorption of H_2O; (ii) The strong metal-support interaction in Pt-O-Ni bonds could optimize the electronic structure and achieve fast electronic transfer; (iii) Superhydrophilic surface could ensure rapid release of gases at a high current density, and then improving HER activity. Actually, the activity of Pt2/Ni(OH)$_2$/NF in 1.0 M KOH was better than the activity in alkaline seawater, which may be caused by due to the critical issue of Cl^- contamination on the Pt surface. Therefore, the cyclic voltammetry at 0.7–0.8 V were tested in Fig. S8, Pt2/Ni(OH)$_2$/NF had a larger ECSA in 1.0 M KOH than that in alkaline seawater [37]. This meant that Cl^- contamination on the Pt

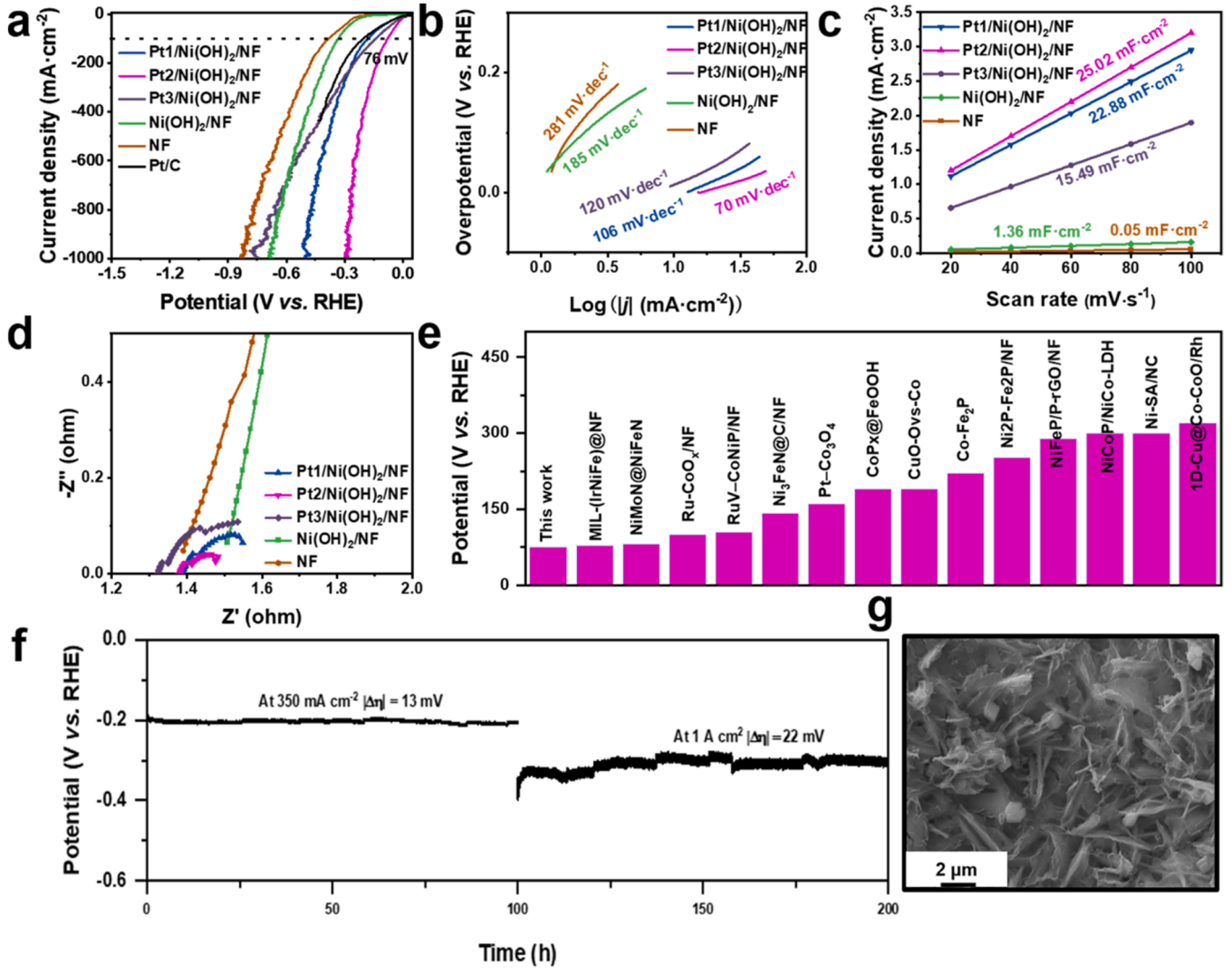

Fig. 3. (a) LSV curves. (b) Tafel plots. (c) Electrochemical double layer capacitance (C_{dl}). (d) EIS. (e) Performance comparison diagram. (f) Long-term stability measurements. (g) SEM image after stability tests.

surface in alkaline splitting could lower the active area and then affect the activity of Pt2/Ni(OH)$_2$/NF. The double-layer capacitance (C_{dl}) for Pt2/Ni(OH)$_2$/NF was 25.02 mF·cm^{-2} in Fig. 3c. This meant that the catalyst had a high ECSA to expose more reactive sites. In addition, the Nyquist diagram (Fig. 3d) of Pt2/Ni(OH)$_2$/NF was the smallest among samples, which further indicated that faster charge transfer and promoted hydrogen evolution kinetics after introduction of Pt nanoparticles and Ov. More importantly, compared to other recently reported seawater-based electrocatalysts in Fig. 3e, Pt2/Ni(OH)$_2$/NF also delivered excellent HER property from the aspect of overpotential at 100 mA cm^{-2}. Furthermore, catalytic stability was carried out by amperometric stability for 200 h (Fig. 3f). Actually, there was negligible changes due to the strong Pt-O-Ni interaction. And SEM and XRD images (Fig. 3g and S9) of Pt2/Ni(OH)$_2$/NF after stability tests also showed its morphological features and phase structure, it could be seen that Pt2/Ni(OH)$_2$/NF was transformed into rough due to the long time surface reactions in alkaline seawater. Such result meant Pt2/Ni(OH)$_2$/NF had high structural and catalytic robustness and application prospect in

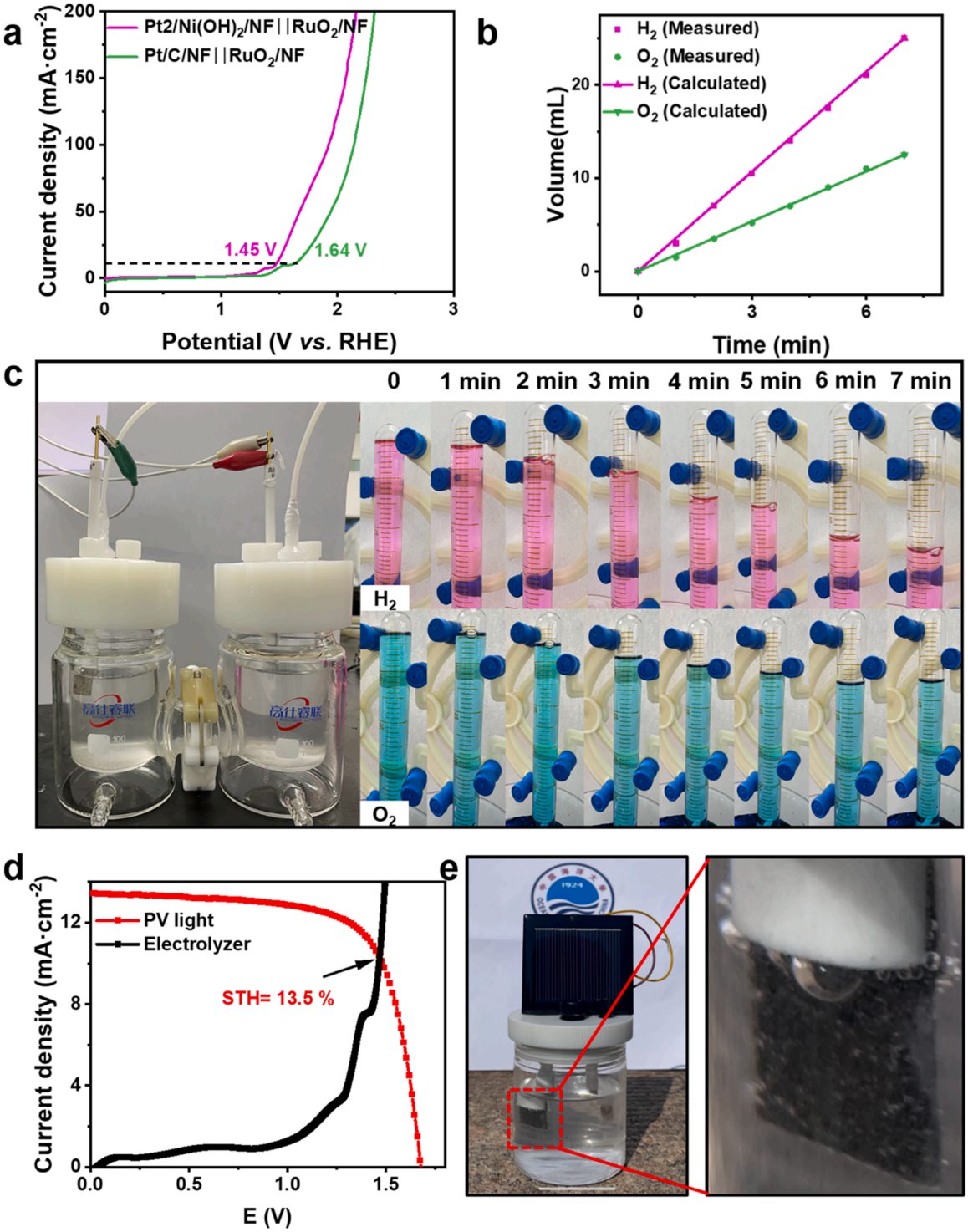

Fig. 4. (a) LSV curves. (b) Device diagram for measuring Faraday efficiency. (c) Enlargement of a drainage device in seawater media. (d) Current density–potential curves of the seawater electrolyzer and PSC. (e) Typical picture exhibiting the generation of H_2 gas during overall seawater splitting under natural light.

seawater splitting due to the SMSI effect at interface.

3.3. Overall seawater-splitting measurement

A seawater splitting cell was constructed by using Pt2/Ni(OH)$_2$/NF as cathode material and bare RuO_2/NF as anode material in Fig. S10. Compared with Pt/C/NF= |RuO_2/NF (1.64 V) in alkaline seawater, Pt2/Ni(OH)$_2$/NF electrolyzer merely required 1.45 V at 10 mA cm^{-2} (Fig. 4a). Additionally, the Faraday efficiency (FE) was tested using the drainage method in Fig. 4b and H-type electrolytic cell was used to collect H_2 and O_2 in Fig. 4c. Fig. 4b proved that the FE was nearly 100%, indicating that catalysts had high selectivity in electrocatalytic seawater splitting [38]. Furthermore, Fig. 4d showed the photo-driven water--splitting system under simulated AM 1.5 G (intensity: 100 mW cm^{-2}) illumination. In order to obtain sufficient photovoltage for seawater electrolysis, two perovskite solar cells (PSC) were connected in series and connected with Pt2/Ni(OH)$_2$/NF electrolytic cells to form a solar-driven electrolytic system. Fig. 4d showed a solar to hydrogen (STH) efficiency as high as 13.5% in alkaline seawater splitting [39]. This result was better than that of coupled normal Si solar cell (Fig. S11), and even higher than most of other reported works in Table 1. By coupling solar cell with the electrolyzer, many bubbles could be seen under natural light (actual voltage was 1.71 V) in Fig. 4e and S12 [26, 40]. Based on electrocatalytic testing results, Pt2/Ni(OH)$_2$/NF revealed excellent catalytic performance from the aspects of activity and the stability in alkaline seawater splitting for hydrogen production, which were capable for AEM electrolyzer.

3.4. AEM electrolyzer measurement

To realize the high-efficiency hydrogen production in industry, AEM electrolyzer were assembled. Pt2/Ni(OH)$_2$/NF as cathode material in AEM water electrolyzer were used to verify their performance in practical devices [41–43]. The components inside the AEM water electrolyzer were shown in Fig. 5a. Here, alkaline exchange membranes were used in our device. As nickel-based materials were stable and mostly used as anode and cathode catalysts in industry. Bare NF materials were used as electrodes for comparison. AEM water electrolyzer had a significant H_2/O_2 bubble formation as shown in Fig. 5b. At the flow rate of the electrolyte of 30 mL·min^{-1}, AEM electrolyzer with Pt2/Ni(OH)$_2$/NF cathode catalyst was only 1.46 V at 10 mA cm^{-2} and 1.60 V for the unit with the bare NF (Fig. 5c). Hydrogen production rate was calculated as1425 L·h^{-1}, and the energy consumption to produce 1 m^3 of H_2 was 3.8 kW·h, which was lower than NF= |NF (4.3 kW·h) at the current density of 200 mA·cm^{-2} (Fig. 5d). The above results further confirmed the excellent activity of as-prepared Pt2/Ni(OH)$_2$/NF in electrocatalytic applications in practice.

3.5. Density functional theory (DFT) calculations

DFT calculations were applied to investigate the intrinsic electronic structure to study intrinsic activity of Pt2/Ni(OH)$_2$/NF. Localized charge distribution in Ov-Pt/Ni(OH)$_2$ model was simulated to study the strong metal-support interaction of Pt-O-Ni bonds of Pt2/Ni(OH)$_2$/NF [44]. Obviously, affected by the SMSI effect of Pt-O-Ni bonds, the localized charge distribution (Fig. 6a and 6b) of Pt/Ni(OH)$_2$ and Ov-Pt/Ni(OH)$_2$ underwent a symmetry breaking charge transfer in Ni(OH)$_2$ at the interface. This would result in a non-uniform charge distribution and electron redistribution [45]. Notably, unlike Pt/Ni(OH)$_2$, the generation of Ov led to the aggregation of electrons on adjacent Ni atoms in red circle, which optimized its H* adsorption ability. And electron aggregation on Pt nanoparticles due to SMSI effect of Pt-O-Ni bonds could

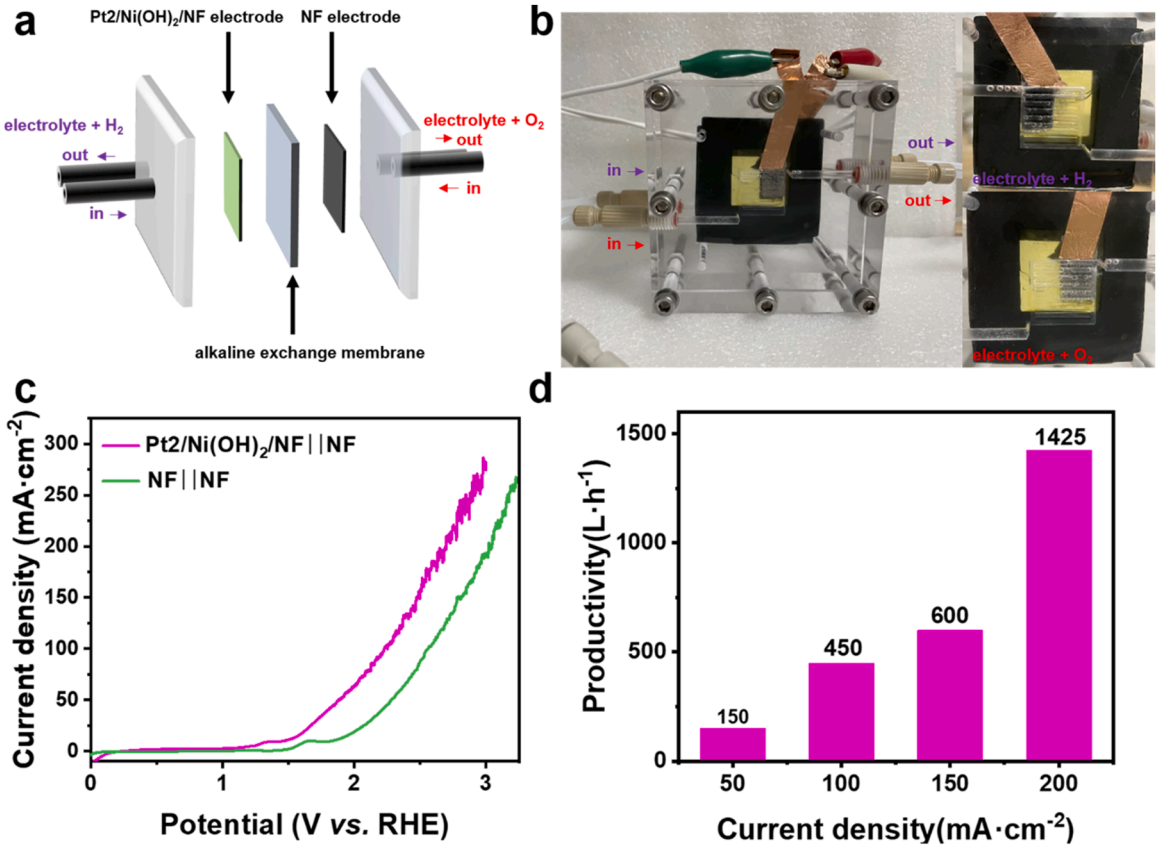

Fig. 5. (a) Schematic picture of AEM water electrolyzer. (b) Typical picture of AEM water electrolyzer. (c) LSV curves of the electrolyzer (without iR compensation). (d) Plot of calculated hydrogen production of Pt2/Ni(OH)$_2$/NF.

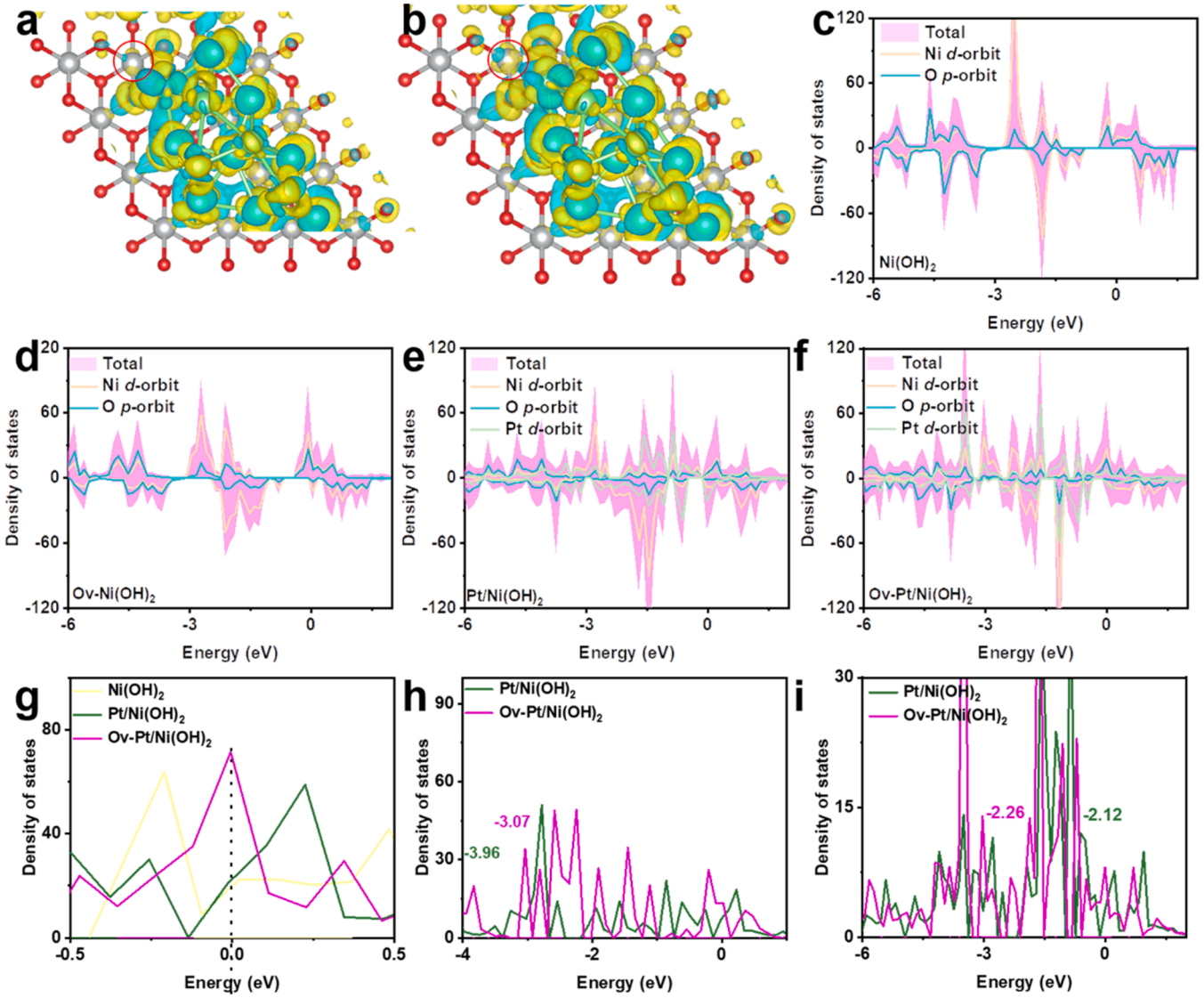

Fig. 6. Atomic models with charge density difference plot of (a) $Pt/Ni(OH)_2$ and (b) $Ov\text{-}Pt/Ni(OH)_2$. DOS of (c) $Ni(OH)_2$, (d) $Ov\text{-}Ni(OH)_2$, (e) $Pt/Ni(OH)_2$ and (f) $Ov\text{-}Pt/Ni(OH)_2$. (g) TDOS. D-band centers of (h) Ni atoms and (i) Pt atoms.

promote the adsorption of H* . The schematic models were calculated in Fig. S13. As displayed in Figs. 6c - 6f, it could be seen that SMSI effect of Pt-O-Ni bonds, and Ov could effectively change the electronic structure of $Ni(OH)_2$ due to its metallic character with zero bandgap. Of note, after forming SMSI and Ov, total DOS (TDOS) of $Ov\text{-}Pt/Ni(OH)_2$ at the Fermi level was higher than that of $Pt/Ni(OH)_2$ and $Ni(OH)_2$ (Fig. 6g). Such result suggested strong interaction in Pt-O-Ni could efficiently achieve the fast electrons transfer rate and enhance electrical conductivity [46].

Moreover, *d*-band center was used to reflect the electronic interactions between the adsorbate and metal [47,48]. Compared with that of $Pt/Ni(OH)_2$ (−3.96 eV), *d*-band center of Ni was − 3.07 eV ($Ov\text{-}Pt/Ni(OH)_2$) in Fig. 6h. Notably, the formation of Pt nanoparticles could increase the D-band central energy level and lead to the strong Ni-H interaction, improving electrocatalytic activity. Fig. 6i also proved that the presence of Ov could weaken the H* adsorption on Pt sites. In short, the strong interaction in $Ov\text{-}Pt/Ni(OH)_2$ can effectively regulate H* adsorption and desorption on active sites, and then and optimize its intrinsic HER performance [49].

The ΔG_{H^*} was applied for in-depth prediction of the synergy of Pt nanoparticles and Ov. Of note, when ΔG_{H^*} was close to 0, it meant that catalyst had a superior H* adsorption capacity [50]. From Fig. 7 and S14, the ΔG_{H^*} value (−0.50 eV) at the Pt2 site in $Pt/Ni(OH)_2$ was better than that at the Pt1 site (−0.63 eV) and O site (−0.69 eV), suggested that the adsorption activity of the H* intermediate in $Pt/Ni(OH)_2$ was stronger at the Pt2 site than other sites. Meantime, the introduction of Pt nanoparticles greatly improved ΔG_{H^*} (−1.07 eV) of $Ni(OH)_2$. Furthermore, the adsorption energy had a minimum of − 0.20 eV in all samples after the formation of Ov in $Pt/Ni(OH)_2$, which indicated that the synergistic effect of Pt-Ov sites could effectively regulate H* adsorption and promote H_2 release.

Recently, hydrogen spillover as a novel method to regulate the activity had been widely studied [51,52]. When the ΔG_{H^*} value of active site (M) was more negative, the M-H adsorption was stronger. Otherwise, the M-H adsorption was weaker. Therefore, when H* adsorption from the active site was stronger to weaker, it meant that H_2 was easy to spill out. The free energy values of HER on the Pt sites and O sites through the hydrogen-spillover pathway was summarized in Fig. 8a. Firstly, It could be seen that ΔG_{H2O} on the $Ov\text{-}Pt/Ni(OH)_2$ surface (−0.51 eV) was obviously lower than that on the $Pt/Ni(OH)_2$ surface (−0.49 eV), suggesting Ov could achieve high-efficiency adsorption of H_2O, which was beneficial to promote above Volmer process ($H_2O + e^- = H^* + OH^-$). And then, ΔG_{H^*} value (−0.50 eV) of Pt2 sites in $Pt/Ni(OH)_2$ was closer to zero than other sites, which implied Pt2 sites were most active sites. If H could be transferred to Pt nanoparticles across the

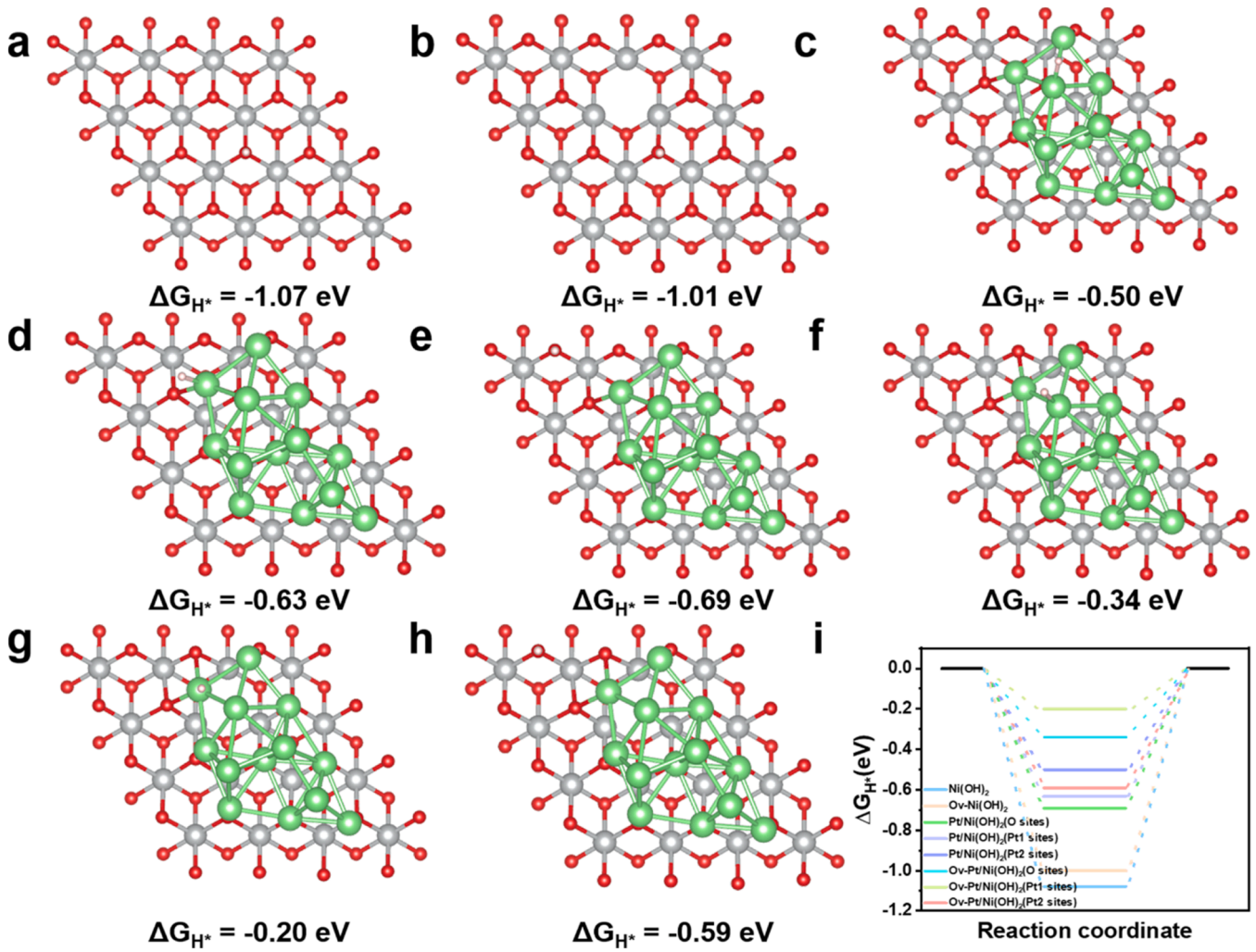

Fig. 7. The top-view schematic models of (a) Ni(OH)$_2$-O sites, (b) Ov-Ni(OH)$_2$-O sites, (c) Pt/Ni(OH)$_2$- Pt2 sites, (d) Pt/Ni(OH)$_2$-Pt1 sites, (e) Pt/Ni(OH)$_2$-O sites, (f) Ov-Pt/Ni(OH)$_2$- Pt2 sites, (g) Ov-Pt/Ni(OH)$_2$-Pt1 sites and (h) Ov-Pt/Ni(OH)$_2$-O sites. (i) ΔG$_{H^*}$.

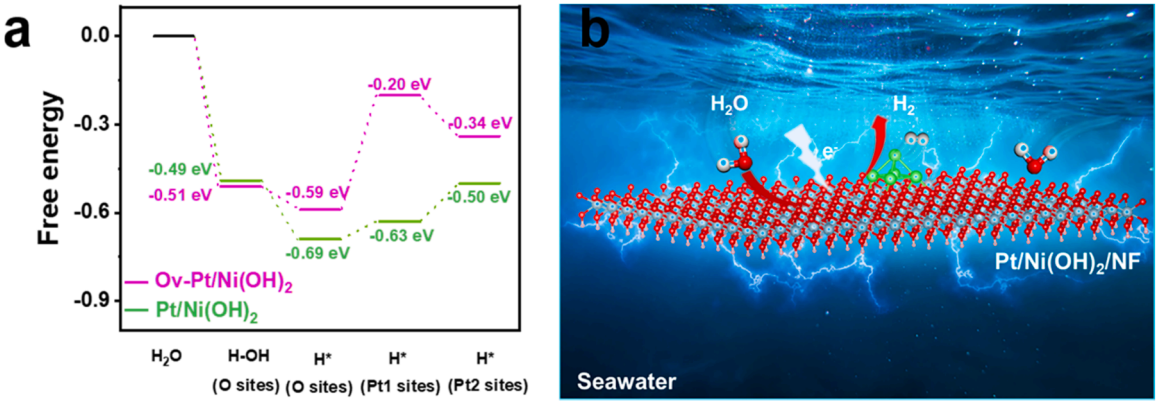

Fig. 8. (a) Calculated adsorption free energy diagrams onto the Pt/Ni(OH)$_2$ and Ov-Pt/Ni(OH)$_2$. (b) Reaction kinetic mechanism diagram.

edge of Ni(OH)$_2$ surface, initial proton adsorption and final H$_2$ desorption would be easily occurred in HER. After Ov formation, it can be seen that the Pt1 site replaced the Pt2 site as the most active site. Meantime, the ΔG$_{H^*}$ value of Pt1 site in Ov-Pt/Ni(OH)$_2$ was − 0.20 eV, which was closer to zero than Pt2 sites in Pt/Ni(OH)$_2$ and suggested Ov would greatly promote hydrogen spill-over, and then achieve efficient HER activity. In conclusion, the synergistic effect of Pt-Ov sites can effectively regulate the localized charge density, and then balance the adsorption and desorption of H* . Based on the above research, reaction kinetic mechanism diagram were showed in Fig. 8b. Notably, H$_2$O preferentially adsorbed on the surface of Ni(OH)$_2$ and decomposed to produce H$^+$, which would gain electrons. Finally, H* spilled from Ni(OH)$_2$ and transfers to Pt surface, and then become H$_2$.

4. Conclusion

In summary, we reported a novel MOF derived nanosheets-nanoparticle-structured Pt2/Ni(OH)$_2$/NF, which has abundant O vacancies, SMSI at interface and excellent superhydrophilic surface. Pt2/Ni(OH)$_2$/NF showed excellent HER performance, requiring merely 283 mV at 1000 mA cm^{-2}, which was even much better than Pt/C catalyst materials. Meanwhile, benefitting from the strong interaction of Pt-O-Ni, the catalyst also showed high stability for 200 h. Assembling our electrodes with a photovoltaic cell yielded up to 13.5% STH conversion efficiency. And the cell voltage for the AEM seawater electrolyzer with the Pt2/Ni(OH)$_2$/NF cathode was 1.46 V at 10 A cm^{-2}. Corresponding power consumption of Pt2/Ni(OH)$_2$/NF= |NF was 3.8 kW·h, below that of NF= |NF (4.3 kW·h) under 200 mA·cm^{-2}. DFT calculation showed synergistic effect of SMSI of Pt-O-Ni bonds and Ov could effectively regulate the localized charge density and electronic structure. Pt nanoparticles and Ov could balance H* adsorption and desorption and optimize hydrogen spillover from Ni(OH)$_2$ to Pt sites.

CRediT authorship contribution statement

Jianpeng Sun: Conceptualization, Methodology, Investigation, Writing – original draft preparation, Writing – review & editing. **Zisheng Zhang**: Methodology, Investigation, Writing – review & editing. **Xiangchao Meng**: Supervision, Conceptualization, Writing – original draft, Writing – review & editing.

Declaration of Competing Interest

The authors declare that they have no known competing financial interests or personal relationships that could have appeared to influence the work reported in this paper.

Data availability

Data will be made available on request.

Acknowledgements

X.M. acknowledges the financial supports from National Natural Science Foundation of China (Grant No: 22002146) and Taishan Scholars Foundation of Shandong province (No.: tsqn201909058). The authors would like to thank Shiyanjia Lab (https://www.shiyanjia.com) for the XRD, SEM, XPS etc. analysis.

Appendix A. Supporting information

Supplementary data associated with this article can be found in the online version at doi:10.1016/j.apcatb.2023.122703.

References

[1] L. Guo, J. Chi, J. Zhu, T. Cui, J. Lai, L. Wang, Dual-doping $NiMoO_4$ with multi-channel structure enable urea-assisted energy-saving H_2 production at large current density in alkaline seawater, Appl. Catal. B: Environ. 320 (2023) 121977–121986, https://doi.org/10.1016/j.apcatb.2022.121977.

[2] F.S. Hegner, F.A. Garcés-Pineda, J. González-Cobos, B. Rodríguez-García, M. Torréns, E. Palomares, N. López, J.-R. Galán-Mascarós, Understanding the catalytic selectivity of cobalt hexacyanoferrate toward oxygen evolution in seawater electrolysis, ACS Catal. 11 (2021) 13140–13148, https://doi.org/10.1021/acscatal.1c03502.

[3] S. Dresp, F. Dionigi, M. Klingenhof, P. Strasser, Direct electrolytic splitting of seawater: opportunities and challenges, ACS Energy Lett. 4 (2019) 933–942, https://doi.org/10.1021/acsenergylett.9b00220.

[4] L. Yu, Q. Zhu, S. Song, B. McElhenny, D. Wang, C. Wu, Z. Qin, J. Bao, Y. Yu, S. Chen, Z. Ren, Non-noble metal-nitride based electrocatalysts for high-performance alkaline seawater electrolysis, Nat. Commun. 10 (2019) 5106–5115, https://doi.org/10.1038/s41467-019-13092-7.

[5] C. Qian, W. Shao, X. Zhang, X. Mu, X. Gu, M. Yu, L. Ma, S. Liu, S. Mu, Competitive coordination-pairing between Ru clusters and single-atoms for efficient hydrogen evolution reaction in alkaline seawater, Small 18 (2022) 2204155–2204163, https://doi.org/10.1002/smll.202204155.

[6] H. Jin, X. Wang, C. Tang, A. Vasileff, L. Li, A. Slattery, S.Z. Qiao, Stable and highly efficient hydrogen evolution from seawater enabled by an unsaturated nickel surface nitride, Adv. Mater. 33 (2021), e2007508, https://doi.org/10.1002/adma.202007508.

[7] B. Zhang, S. Liu, S. Zhang, Y. Cao, H. Wang, C. Han, J. Sun, High corrosion resistance of NiFe-layered double hydroxide catalyst for stable seawater electrolysis promoted by phosphate intercalation, Small (2022), e2203852, https://doi.org/10.1002/smll.202203852.

[8] X. Wang, X. Zhou, C. Li, H. Yao, C. Zhang, J. Zhou, R. Xu, L. Chu, H. Wang, M. Gu, H. Jiang, M. Huang, Asymmetric Co-N_3P_1 trifunctional catalyst with tailored electronic structures enabling boosted activities and corrosion resistance in uninterrupted seawater splitting system, Adv. Mater. (2022) 2204021–2204033, https://doi.org/10.1002/adma.202204021.

[9] W. Zang, T. Sun, T. Yang, S. Xi, M. Waqar, Z. Kou, Z. Lyu, Y.P. Feng, J. Wang, S. J. Pennycook, Efficient hydrogen evolution of oxidized Ni-N_3 defective sites for alkaline freshwater and seawater electrolysis, Adv. Mater. 33 (2021), e2003846, https://doi.org/10.1002/adma.202003846.

[10] Tu Haq, M. Pasha, Y. Tong, S.A. Mansour, Y. Haik, Au nanocluster coupling with Gd-Co_2B nanoflakes embedded in reduced TiO_2 nanosheets: Seawater electrolysis at low cell voltage with high selectivity and corrosion resistance, Appl. Catal. B: Environ. 301 (2022) 120836–120849, https://doi.org/10.1016/j.apcatb.2021.120836.

[11] J. Dong, X. Zhang, J. Huang, J. Hu, Z. Chen, Y. Lai, In-situ formation of unsaturated defect sites on converted CoNi alloy/Co-Ni LDH to activate MoS_2 nanosheets for pH-universal hydrogen evolution reaction, Chem. Eng. J. 412 (2021) 128556–128564, https://doi.org/10.1016/j.cej.2021.128556.

[12] B. Wang, S. Jiao, Z. Wang, M. Lu, D. Chen, Y. Kang, G. Pang, S. Feng, Rational design of NiFe LDH@Ni_3N nano/microsheet arrays as a bifunctional electrocatalyst for overall water splitting, J. Mater. Chem. A 8 (2020) 17202–17211, https://doi.org/10.1039/D0TA01966F.

[13] Y. Zhu, X. Wang, X. Zhu, Z. Wu, D. Zhao, F. Wang, D. Sun, Y. Tang, H. Li, G. Fu, Improving the oxygen evolution activity of layered double-hydroxide via erbium-induced electronic engineering, Small (2022), e2206531, https://doi.org/10.1002/smll.202206531.

[14] L. Xie, X. Ren, Q. Liu, G. Cui, R. Ge, A.M. Asiri, X. Sun, Q. Zhang, L. Chen, A. Ni, $OH)_2$–PtO_2 hybrid nanosheet array with ultralow Pt loading toward efficient and durable alkaline hydrogen evolution, J. Mater. Chem. A 6 (2018) 1967–1970, https://doi.org/10.1039/C7TA09990H.

[15] T. Ma, H. Cao, S. Li, S. Cao, Z. Zhao, Z. Wu, R. Yan, C. Yang, Y. Wang, P.A. van Aken, L. Qiu, Y.G. Wang, C. Cheng, Crystalline lattice-confined atomic pt in metal carbides to match electronic structures and hydrogen evolution behaviors of platinum, Adv. Mater. (2022) 2206368–2206378, https://doi.org/10.1002/adma.202206368.

[16] K.L. Zhou, Z. Wang, C.B. Han, X. Ke, C. Wang, Y. Jin, Q. Zhang, J. Liu, H. Wang, H. Yan, Platinum single-atom catalyst coupled with transition metal/metal oxide heterostructure for accelerating alkaline hydrogen evolution reaction, Nat. Commun. 12 (2021) 3783–3792, https://doi.org/10.1038/s41467-021-24079-8.

[17] Y. Shi, D. Zhang, H. Huang, H. Miao, X. Wu, H. Zhao, T. Zhan, X. Chen, J. Lai, L. Wang, Mixture phases engineering of PtFe nanofoams for efficient hydrogen evolution, Small 18 (2022) 2106947–2106954, https://doi.org/10.1002/smll.202106947.

[18] K. Xiang, Z. Song, D. Wu, X. Deng, X. Wang, W. You, Z. Peng, L. Wang, J.-L. Luo, X.-Z. Fu, Bifunctional Pt–Co_3O_4 electrocatalysts for simultaneous generation of hydrogen and formate via energy-saving alkaline seawater/methanol co-electrolysis, J. Mater. Chem. A 9 (2021) 6316–6324, https://doi.org/10.1039/D0TA10501E.

[19] D. Li, F. Liu, J. Dou, Q. Zhao, Pt decorated Ni−Ni(OH)$_2$ nanotube arrays for efficient hydrogen evolution reaction, Chemcatchem 13 (2021) 5078–5083, https://doi.org/10.1002/cctc.202101382.

[20] A. Kong, M. Peng, M. Liu, Y. Lv, H. Zhang, Y. Gao, J. Liu, Y. Fu, W. Li, J. Zhang, Robust Pt/TiO_2/Ni(OH)$_2$ nanosheet arrays enable outstanding performance for high current density alkaline water electrolysis, Appl. Catal. B: Environ. 316 (2022) 121654–121664, https://doi.org/10.1016/j.apcatb.2022.121654.

[21] Z. Luo, G. Zhao, H. Pan, W. Sun, Strong metal–support interaction in heterogeneous catalysts, Adv. Energy Mater. 12 (2022) 2201395–2201409, https://doi.org/10.1002/aenm.202201395.

[22] X. Mu, X. Gu, S. Dai, J. Chen, Y. Cui, Q. Chen, M. Yu, C. Chen, S. Liu, S. Mu, Breaking the symmetry of single-atom catalysts enables an extremely low energy barrier and high stability for large-current-density water splitting, Energy Environ. Sci. 15 (2022) 4048–4057, https://doi.org/10.1039/D2EE01337A.

[23] X. Wu, Z. Wang, D. Zhang, Y. Qin, M. Wang, Y. Han, T. Zhan, B. Yang, S. Li, J. Lai, L. Wang, Solvent-free microwave synthesis of ultra-small Ru-Mo_2C@CNT with strong metal-support interaction for industrial hydrogen evolution, Nat. Commun. 12 (2021) 4018–4027, https://doi.org/10.1038/s41467-021-24322-2.

[24] B. Zhang, Y. Zheng, T. Ma, C. Yang, Y. Peng, Z. Zhou, M. Zhou, S. Li, Y. Wang, C. Cheng, Designing MOF nanoarchitectures for electrochemical water splitting, Adv. Mater. 33 (2021) 2006042–2130378, https://doi.org/10.1002/adma.202006042.

[25] Z. Huang, S. Yuan, T. Zhang, B. Cai, B. Xu, X. Lu, L. Fan, F. Dai, D. Sun, Selective selenization of mixed-linker Ni-MOFs: $NiSe_2$@NC core-shell nano-octahedrons with tunable interfacial electronic structure for hydrogen evolution reaction, Appl. Catal. B: Environ. 272 (2020) 118976–118983, https://doi.org/10.1016/j.apcatb.2020.118976.

[26] Y. Wu, Z. Tian, S. Yuan, Z. Qi, Y. Feng, Y. Wang, R. Huang, Y. Zhao, J. Sun, W. Zhao, W. Guo, J. Feng, J. Sun, Solar-driven self-powered alkaline seawater electrolysis via multifunctional earth-abundant heterostructures, Chem. Eng. J. 411 (2021) 128538–128547, https://doi.org/10.1016/j.cej.2021.128538.
[27] K. Rui, G. Zhao, M. Lao, P. Cui, X. Zheng, X. Zheng, J. Zhu, W. Huang, S.X. Dou, W. Sun, Direct hybridization of noble metal nanostructures on 2D metal-organic framework nanosheets to catalyze hydrogen evolution, Nano Lett. 19 (2019) 8447–8453, https://doi.org/10.1021/acs.nanolett.9b02729.
[28] J. Song, S. Zhao, D. Liu, Y. Xiong, F. Hu, L. Li, L. Li, H. Pan, S. Peng, Plasma-induced defect engineering of porous metal-organic framework nanosheet arrays for efficient water splitting, Chem. Commun. 58 (2022) 9662–9665, https://doi.org/10.1039/D2CC03633A.
[29] Y. Huang, M. Li, F. Pan, Z. Zhu, H. Sun, Y. Tang, G. Fu, Plasma-induced Mo-doped Co_3O_4 with enriched oxygen vacancies for electrocatalytic oxygen evolution in water splitting, Carbon Energy (2022) 1–14, https://doi.org/10.1002/cey2.279.
[30] Z. Xiao, Y. Mei, S. Yuan, H. Mei, B. Xu, Y. Bao, L. Fan, W. Kang, F. Dai, R. Wang, L. Wang, S. Hu, D. Sun, H.C. Zhou, Controlled hydrolysis of metal-organic frameworks: Hierarchical Ni/Co-layered double hydroxide microspheres for high-performance supercapacitors, ACS Nano 13 (2019) 7024–7030, https://doi.org/10.1021/acsnano.9b02106.
[31] X. Xu, C. Zhang, J. Li, H. Liu, G. Su, Z. Shi, M. Huang, Redistributing interfacial charge density of $Ni_{12}P_5/Ni_3P$ via Fe doping for ultrafast urea oxidation catalysis at large current densities, Chem. Eng. J. 452 (2023) 139362–139370, https://doi.org/10.1016/j.cej.2022.139362.
[32] R. Andaveh, G. Barati Darband, M. Maleki, A. Sabour Rouhaghdam, Superaerophobic/superhydrophilic surfaces as advanced electrocatalysts for the hydrogen evolution reaction: a comprehensive review, J. Mater. Chem. A 10 (2022) 5147–5173, https://doi.org/10.1039/D1TA10519A.
[33] Y. Mei, H. Li, Y. Cong, S. Huang, W. Xu, J. Qian, T.-T. Li, Self-supported N-doped carbon@$NiXCo_2$-XP core-shell nanorod arrays on 3D Ni foam for boosted hydrogen evolution reaction, Int. J. Hydrog. Energy 46 (2021) 36046–36055, https://doi.org/10.1016/j.ijhydene.2021.08.171.
[34] B. Zhou, Y. Li, Y. Zou, W. Chen, W. Zhou, M. Song, Y. Wu, Y. Lu, J. Liu, Y. Wang, S. Wang, Platinum modulates redox properties and 5-hydroxymethylfurfural adsorption kinetics of $Ni(OH)_2$ for biomass upgrading, Angew. Chem. Int. Ed. 60 (2021) 22908–22914, https://doi.org/10.1002/anie.202109211.
[35] S. Cai, L. Wang, S. Heng, H. Li, Y. Bai, D. Dang, Q. Wang, P. Zhang, C. He, Interaction of single-atom platinum−oxygen vacancy defects for the boosted photosplitting water H_2 evolution and CO_2 photoreduction: Experimental and theoretical study, The, J. Phys. Chem. 124 (2020) 24566–24579, https://doi.org/10.1021/acs.jpcc.0c04931.
[36] W. Yang, S. Chen, Recent progress in electrode fabrication for electrocatalytic hydrogen evolution reaction: a mini review, Chem. Eng. J. 393 (2020) 124726–124739, https://doi.org/10.1016/j.cej.2020.124726.
[37] H. Li, H. Wang, W. Qian, S. Zhang, S. Wessel, T.T.H. Cheng, J. Shen, S. Wu, Chloride contamination effects on proton exchange membrane fuel cell performance and durability, J. Power Sources 196 (2011) 6249–6255, https://doi.org/10.1016/j.jpowsour.2011.04.018.
[38] J. Sun, Z. Huang, T. Huang, X. Wang, X. Wang, P. Yu, C. Zong, F. Dai, D. Sun, Defect-rich porous $CoS_{1.097}/MoS_2$ hybrid microspheres as electrocatalysts for pH-universal hydrogen evolution, Acs Appl. Energy Mater. 2 (2019) 7504–7511, https://doi.org/10.1021/acsaem.9b01486.
[39] C. Wang, M. Zhu, Z. Cao, P. Zhu, Y. Cao, X. Xu, C. Xu, Z. Yin, Heterogeneous bimetallic sulfides based seawater electrolysis towards stable industrial-level large current density, Appl. Catal. B: Environ. 291 (2021) 120071–120078, https://doi.org/10.1016/j.apcatb.2021.120071.
[40] J. Lee, H. Jung, Y.S. Park, N. Kwon, S. Woo, N.C.S. Selvam, G.S. Han, H.S. Jung, P. J. Yoo, S.M. Choi, J.W. Han, B. Lim, Chemical transformation approach for high-performance ternary NiFeCo metal compound-based water splitting electrodes, Appl. Catal. B: Environ. 294 (2021) 120246–120354, https://doi.org/10.1016/j.apcatb.2021.120246.
[41] S. Du, R. Chen, W. Chen, H. Gao, J. Jia, Z. Xiao, C. Xie, H. Li, L. Tao, J. Huo, Y. Wang, S. Wang, Activation of iridium site by anchoring ruthenium atoms on defects for efficient anodic catalyst in polymer electrolyte membrane water electrolyzers, J. Energy Chem. 75 (2022) 260–266, https://doi.org/10.1016/j.jechem.2022.08.020.
[42] X. Yan, J. Biemolt, K. Zhao, Y. Zhao, X. Cao, Y. Yang, X. Wu, G. Rothenberg, N. Yan, A membrane-free flow electrolyzer operating at high current density using earth-abundant catalysts for water splitting, Nat. Commun. 12 (2021) 4143, https://doi.org/10.1038/s41467-021-24284-5.
[43] F. Sun, J. Qin, Z. Wang, M. Yu, X. Wu, X. Sun, J. Qiu, Energy-saving hydrogen production by chlorine-free hybrid seawater splitting coupling hydrazine degradation, Nat. Commun. 12 (2021) 4182–4192, https://doi.org/10.1038/s41467-021-24529-3.
[44] Y. Liu, Q. Feng, W. Liu, Q. Li, Y. Wang, B. Liu, L. Zheng, W. Wang, L. Huang, L. Chen, X. Xiong, Y. Lei, Boosting interfacial charge transfer for alkaline hydrogen evolution via rational interior Se modification, Nano Energy 81 (2021), 105641, https://doi.org/10.1016/j.nanoen.2020.105641.
[45] C. Li, Z. Wang, M. Liu, E. Wang, B. Wang, L. Xu, K. Jiang, S. Fan, Y. Sun, J. Li, K. Liu, Ultrafast self-heating synthesis of robust heterogeneous nanocarbides for high current density hydrogen evolution reaction, Nat. Commun. 13 (2022) 3338–3348.
[46] Z. Li, S. Xin, Y. Zhang, Z. Zhang, C. Li, C. Li, R. Bao, J. Yi, M. Xu, J. Wang, Boosting elementary steps kinetics towards energetic alkaline hydrogen evolution via dual sites on phase-separated Ni–Cu–Mn/hydroxide, Chem. Eng. J. 451 (2023) 138540–138548, https://doi.org/10.1016/j.cej.2022.138540.
[47] Z. Lin, B. Xiao, M. Huang, L. Yan, Z. Wang, Y. Huang, S. Shen, Q. Zhang, L. Gu, W. Zhong, Realizing negatively charged metal atoms through controllable d-electron transfer in ternary $Ir_{1-x}Rh_xSb$ intermetallic alloy for hydrogen evolution reaction, Adv. Energy Mater. 12 (2022) 2200855–2200861, https://doi.org/10.1002/aenm.202200855.
[48] D. Wang, X. Jiang, Z. Lin, X. Zeng, Y. Zhu, Y. Wang, M. Gong, Y. Tang, G. Fu, Ethanol-induced hydrogen insertion in ultrafine IrPdH boosts pH-universal hydrogen evolution, Small 18 (2022), e2204063, https://doi.org/10.1002/smll.202204063.
[49] S. Shen, Z. Wang, Z. Lin, K. Song, Q. Zhang, F. Meng, L. Gu, W. Zhong, Crystalline-amorphous interfaces coupling of $CoSe_2$/CoP with optimized d-band center and boosted electrocatalytic hydrogen evolution, Adv. Mater. 34 (2022) 2110631–2110638, https://doi.org/10.1002/adma.202110631.
[50] J.D. Chen, C.H. Chen, Y.Z. Chen, H.Y. Wang, S.J. Mao, Y. Wang, Improving alkaline hydrogen evolution reaction kinetics on molybdenum carbide: Introducing Ru dopant, J. Catal. 392 (2020) 313–321, https://doi.org/10.1016/j.jcat.2020.10.020.
[51] J. Dai, Y. Zhu, Y. Chen, X. Wen, M. Long, X. Wu, Z. Hu, D. Guan, X. Wang, C. Zhou, Q. Lin, Y. Sun, S.C. Weng, H. Wang, W. Zhou, Z. Shao, Hydrogen spillover in complex oxide multifunctional sites improves acidic hydrogen evolution electrocatalysis, Nat. Commun. 13 (2022) 1189–1198, https://doi.org/10.1038/s41467-022-28843-2.
[52] Z.W. Wei, H.J. Wang, C. Zhang, K. Xu, X.L. Lu, T.B. Lu, Reversed charge transfer and enhanced hydrogen spillover in platinum noclusters anchored on titanium oxide with rich oxygen vacancies boost hydrogen evolution reaction, Angew. Chem. Int. Ed. 60 (2021) 16622–16627, https://doi.org/10.1002/anie.202104856.